Structure formation in the Lemaître-Tolman model

Andrzej Krasiński*

N. Copernicus Astronomical Centre, Polish Academy of Sciences, Bartycka 18, 00 716 Warszawa, Poland

Charles Hellaby[†]

Department of Mathematics and Applied Mathematics, University of Cape Town, Rondebosch 7701, South Africa

Structure formation within the Lemaître-Tolman model is investigated in a general manner. We seek models such that the initial density perturbation within a homogeneous background has a smaller mass than the structure into which it will develop, and the perturbation then accretes more mass during evolution. This is a generalization of the approach taken by Bonnor in 1956. It is proved that any two spherically symmetric density profiles specified on any two constant time slices can be joined by a Lemaître-Tolman evolution, and exact implicit formulas for the arbitrary functions that determine the resulting LT model are obtained. Examples of the process are investigated numerically.

　　　　PACS number(s): 98.80.−k, 98.62.Ai, 98.65.−r

I. INTRODUCTION

Though the Lemaître-Tolman (LT) model has been studied extensively (see [1]), the question of whether galaxies and other modern cosmic structures can grow from small initial perturbations, using this exact inhomogenous cosmological model, has not been clearly answered.

Long ago Bonnor [2] considered a version of the general problem, in which the perturbation consisted of an interior region matched to a Friedmann-Lemaître-Robertson-Walker (Friedmann) exterior, so the initial fluctuation of density included all the dust particles that would enter the future galaxy, and so the outer edge of the perturbation had to be comoving with the (spatially homogeneous) background flow ever after. Because of this, and given the present age of the Universe, the initial fluctuation had to have an amplitude many times larger than a statistical fluctuation could have. However, current matter models, that allow perturbations to grow before recombination, have successfully predicted temperature perturbations in the cosmic microwave background (CMB) of order 10^{-5}.

The very existence of inhomogeneous cosmological models (i.e., spatially inhomogeneous solutions of Einstein's equations with expanding matter), such as the LT [3,4] or Szekeres [5,6] models, shows that non-Friedmannian distributions of density and velocity would have been coded in the big bang and need not be "explained" as statistical fluctuations that appeared within a homogeneous background during evolution. Moreover, since the LT collection of models is labeled by two arbitrary functions of mass, that reduce to specific forms in the Friedmann limit, it follows that the dust Friedmann models are a subset of measure zero within the LT set. Consequently, the Friedmann models are very improbable statistically and, assuming that our physical Universe is homogeneous indeed, one needs to explain how homogeneity might have come about out of inhomogeneous initial data, not the other way around. This is what inflation is believed to have done. However, in this paper we shall accept a high degree of homogeneity at decoupling, and we will determine how fast condensations can grow, once they appear in a homogeneous background.

In this paper we shall relax Bonnor's assumptions, and consider the general case. In particular, we envisage a scenario in which the mass of the initial fluctuation is much smaller than the mass of the condensation into which it will develop, and that it captures more mass during its evolution.[1] The outer edge of the growing condensation will thus not be comoving with the background flow. The calculations, although based on exact formulas, will have to be carried out numerically.

In the following we set $\Lambda = 0$, as its effect is felt primarily at late times over the long range, and so will not strongly affect structure formation. Also, current interpretations of the CMB and supernova data that estimate a non-zero Ω_Λ, should be regarded as provisional, since several reasonable alternatives have been put forward.

II. BASIC PROPERTIES OF THE LEMAÎTRE-TOLMAN MODEL

The Lemaître-Tolman (LT) model [3,4] is a spherically symmetric nonstatic solution of the Einstein equations with a dust source. Its metric is

$$ds^2 = dt^2 - \frac{R_{,r}^2}{1+2E(r)} dr^2 - R^2(t,r)(d\vartheta^2 + \sin^2\vartheta d\varphi^2),$$
(2.1)

where $E(r)$ is an arbitrary function (arising as an integration constant from the Einstein equations), $R_{,r}$ is the derivative of the function $R(t,r)$ by r, and R obeys the equation

---

*Email address: akr@camk.edu.pl

[†]Email address: cwh@maths.uct.ac.za

$$R_{,t}^2 = 2E + 2M/R + \frac{1}{3}\Lambda R^2, \qquad (2.2)$$

where Λ is the cosmological constant. Equation (2.2) is a first integral of one of the Einstein equations, and $M(r)$ is another arbitrary function that arises as integration constant. The matter density is

$$\kappa\rho = \frac{2M_{,r}}{R^2 R_{,r}}, \quad \text{where} \quad \kappa = \frac{8\pi G}{c^4}. \qquad (2.3)$$

In the following, we will assume $\Lambda = 0$. Then Eq. (2.2) can be solved explicitly. The solutions are:
When $E < 0$:

$$R(t,r) = -\frac{M}{2E}(1 - \cos \eta),$$

$$\eta - \sin \eta = \frac{(-2E)^{3/2}}{M}(t - t_B(r)), \qquad (2.4)$$

where η is a parameter. When $E = 0$:

$$R(t,r) = \left[\frac{9}{2}M(t - t_B(r))^2\right]^{1/3}, \qquad (2.5)$$

and when $E > 0$:

$$R(t,r) = \frac{M}{2E}(\cosh \eta - 1),$$

$$\sinh \eta - \eta = \frac{(2E)^{(3/2)}}{M}(t - t_B(r)), \qquad (2.6)$$

where $t_B(r)$ is one more arbitrary function (the bang time). Note that all the formulas given so far are covariant under arbitrary coordinate transformations $r = g(r')$, and so r can be chosen at will. This means one of the three functions $E(r)$, $M(r)$ and $t_B(r)$ can be fixed at our convenience by the appropriate choice of g.

In a general LT model, E may change sign, having both recollapsing and ever-expanding regions. Also the space $t = \text{const}$ with $E(r) < 0$ everywhere is not necessarily closed [and the one with $E(r) > 0$ is not necessarily infinite], see Refs. [7,8].

The Friedmann models are contained in the Lemaître-Tolman class as the limit

$$t_B = \text{const}, \quad |E|^{3/2}/M = \text{const}, \qquad (2.7)$$

and one of the standard radial coordinates for the Friedmann model results if the coordinates in Eqs. (2.4)–(2.6) are chosen so that

$$M = M_0 r^3, \qquad (2.8)$$

where M_0 is an arbitrary constant; so that $E = E_0 r^2$, $E_0 = \text{const}$.

It will be convenient in most of what follows to use $M(r)$ as the radial coordinate [i.e., $r' = M(r)$] because in the structure formation context one does not expect any "necks" or "bellies" where $M_{,r} = 0$, and so $M(r)$ should be a strictly growing function in the whole region under consideration. (See the papers by Barnes and, especially, by Hellaby [9,10] for descriptions of necks. Some properties of a neck appeared also in the paper by Novikov [11].) Then

$$\kappa\rho = 2/(R^2 R_{,M}) \equiv 6/(R^3)_{,M}. \qquad (2.9)$$

We also, in searching for realistic models, prefer LT models that are free of shell crossings [7]. This is not because shells of matter cannot collide, but because the LT comoving description breaks down there.

We shall now apply this model to the problem of structure formation within the exact relativity theory (i.e., without approximations). We believe this question has not been satisfactorily answered so far, and so it deserves to be investigated more thoroughly, both as an important consequence of LT models, and with a view to possible cosmological applications. We seek accreting models in which a small initial fluctuation at decoupling captures more mass during its evolution, thus growing in extent as well as in density contrast.

III. THE EVOLUTION AS A MAPPING FROM AN INITIAL DENSITY TO A FINAL DENSITY

The evolution of the LT model is usually specified by defining the initial conditions—the distributions of the big bang time $t_B(M)$ and of energy $E(M)$, or by specifying e.g. the density $\rho(t_1, R)$ and velocity $R_{,t}(t_1, R)$ at an initial instant $t = t_1$. It is, however, possible, to approach the problem in a different way: to specify the density distributions at two different instants, $t = t_1$ and $t = t_2$, calculate the corresponding $E(M)$ and $t_B(M)$, and in this way obtain a definite model. It is not immediately obvious whether all pairs of density distributions may be connected by an LT evolution of a chosen type; nor whether one can ensure shell crossings do not occur between t_1 and t_2. However, such a mapping from an initial density to a given final density should exist in many cases, especially with a sensible choice of density profiles.

In fact, it will be proven below that any initial value of density at a specific position (r, M const) can be connected to any final value of density at the same position by one of the Lemaître-Tolman evolutions (either $E > 0$, or $E < 0$, or, in an exceptional case, $E = 0$). In the Friedmann limit, any two constant densities can be connected by one of the $k > 0$, $k < 0$ or $k = 0$ Friedmann evolutions.

For definiteness, it will be assumed in the following that the final instant t_2 is later than the initial instant t_1, i.e. $t_2 > t_1$, and that the final density $\rho(t_2, M)$ is smaller than the initial density $\rho(t_1, M)$ at the same M. We thus assume that matter has expanded along every world line, but the proof can be easily adapted to the collapse situation.

A. Hyperbolic regions

Let us consider the LT model with $E > 0$. Let the initial and final density distributions at $t = t_1$ and $t = t_2$ be given by

$$\rho(t_1,M)=\rho_1(M), \quad \rho(t_2,M)=\rho_2(M). \quad (3.1)$$

From Eq. (2.3) we then have, for each of t_1 and t_2,

$$R^3(t_i,M)-R^3_{\text{min}i}=\int_{M_{\text{min}}}^{M}\frac{6}{\kappa\rho_i(M')}dM':=R_i^3(M), \quad i=1,2 \quad (3.2)$$

and $R_2(M)>R_1(M)$ in consequence of $\rho(t_2,M)<\rho(t_1,M)$. In the following we will assume there is an origin where $M=0$ and $R(t_i,0)=0$, so that $R_{\text{min}i}=0=M_{\text{min}}$ is valid.[2] Solving the two parts of Eq. (2.6) for $t(R,r)$ and writing it out for each of (t_1,R_1) and (t_2,R_2) leads to

$$t_B=t_i-\frac{M}{(2E)^{3/2}}[\sqrt{(1+2ER_i/M)^2-1}$$
$$-\text{arcosh}(1+2ER_i/M)], \quad i=1,2 \quad (3.3)$$

and then eliminating t_B between the two versions of Eq. (3.3) we find

$$\sqrt{(1+2ER_2/M)^2-1}-\text{arcosh}(1+2ER_2/M)$$
$$-\sqrt{(1+2ER_1/M)^2-1}+\text{arcosh}(1+2ER_1/M)$$
$$=[(2E)^{3/2}/M](t_2-t_1). \quad (3.4)$$

We shall prove that this equation has one and only one solution $E(M)>0$ (in addition to the trivial solution $E=0$) provided that t_2 and t_1 obey a certain inequality (see below). In fact, the inequality will exclude the $E\le 0$ models.

For ease of calculations, let us denote

$$x:=2E/M^{2/3}, \quad a_i=R_i/M^{1/3}, \quad i=1,2;$$

$$\psi_H(x):=\sqrt{(1+a_2x)^2-1}-\text{arcosh}(1+a_2x)$$
$$-\sqrt{(1+a_1x)^2-1}+\text{arcosh}(1+a_1x)$$
$$-(t_2-t_1)x^{3/2}:=\chi_H(x)-(t_2-t_1)x^{3/2}. \quad (3.5)$$

Our problem is then equivalent to the following question: for what values of the parameters $a_2>a_1$ and $t_2>t_1$ does the equation $\psi_H(x)=0$ have a solution $x\ne 0$? Note that ψ_H has a zero at $x=0$ that the more correct but less convenient $x^{-3/2}\chi_H-(t_2-t_1)$ does not have.

Since $x\ge 0$ and $a_i>0$ by definition, $\psi_H(x)$ and $\chi_H(x)$ are well-defined for any $x\in[0,\infty)$. Note that

$$\lim_{x\to\infty}\frac{\text{arcosh}(1+a_ix)}{\sqrt{(1+a_ix)^2-1}}=\lim_{x\to\infty}\frac{\text{arcosh}(1+a_ix)}{(t_2-t_1)x^{3/2}}=0, \quad (3.6)$$

and so in determining the sign of $\psi_H(x)$ as $x\to\infty$, the arcosh terms can be neglected. Note also

$$\lim_{x\to\infty}\frac{\chi_H(x)}{(t_2-t_1)x^{3/2}}=0. \quad (3.7)$$

Hence, the last term in ψ_H becomes dominant when $x\to+\infty$, and so

$$\lim_{x\to+\infty}\psi_H(x)=-\infty. \quad (3.8)$$

It is easy to see that $\psi_H(0)=0$, but we wish to know whether $\psi_H\to 0^+$ or $\psi_H\to 0^-$ as $x\to 0$. For this purpose, note that

$$\frac{d}{dx}\psi_H(x)=\psi_{H,x}=\sqrt{x}\left[\frac{a_2^{3/2}}{\sqrt{2+a_2x}}-\frac{a_1^{3/2}}{\sqrt{2+a_1x}}-\frac{3}{2}(t_2-t_1)\right], \quad (3.9)$$

from which it follows that

$$\psi_{H,x}(0)=0, \quad \lim_{x\to\infty}\psi_{H,x}=-\infty. \quad (3.10)$$

It is also easy to see that the term in square brackets in Eq. (3.9) is a strictly decreasing function for all $x\in[0,\infty)$, and so it may be equal to zero in at most one point. Since it goes to the negative value $-(3/2)(t_2-t_1)$ when $x\to\infty$, it will have a zero when it is positive at $x=0$, i.e. when

$$t_2-t_1<\frac{\sqrt{2}}{3}(a_2^{3/2}-a_1^{3/2}). \quad (3.11)$$

By comparison with Eq. (2.5), since $a_i=R_i/M^{1/3}$, the above is seen to be equivalent to the statement that between t_1 and t_2, $R(t,M)$ has increased by more than it would have increased in the $E=0$ LT model. This is a necessary condition for the existence of an $E>0$ evolution connecting $R(t_1,M)$ to $R(t_2,M)$.

It is also a sufficient condition, as we now explain. With Eq. (3.11) satisfied, $\lim_{x\to 0}\psi_{H,x}=0^+$, i.e. $\psi_{H,x}>0$ in a neighborhood of $x=0$, then it goes through zero exactly once, at some $x=x_m$, and becomes negative. This means that $\psi_H(x)$ itself is increasing from the value 0 at $x=0$, to a maximum at $x=x_m$, and is then decreasing all the way to $x\to\infty$ where it becomes $-\infty$. Hence, at one and only one $x=x_0>x_m$, $\psi_H(x_0)=0$. This implies that Eq. (3.4) defines a function $E(M)$ in the whole range of M in which Eq. (3.11) is satisfied. Examples of the functions $\psi_H(x)$ from Eq. (3.8) that obey or do not obey Eq. (3.11) are shown in Fig. 1.

There remains a practical problem for the numerical calculation of $E(M)$. Since the range of x is infinite in Eq. (3.5), an initial value $x_A<\infty$ such that $\psi_H(x_A)<0$ has to be determined first. For this purpose, note that for large x we have $\sqrt{(1+a_ix)^2-1}\approx 1+a_ix$. Together with Eq. (3.6), this implies that $\psi_H(x)$ is well approximated for large x by

$$\psi_A(x):=(a_2-a_1)x-(t_2-t_1)x^{3/2}. \quad (3.12)$$

Indeed, it is easy to verify that for all $x>0$

$$\psi_H(x)<\psi_A(x). \quad (3.13)$$

_____

[2]For examples where this is not the case, see the papers by Einstein and Straus [12,13] with $M_{min}\ne 0$ and $R_{min}=0$, and by Bonnor and Chamorro [14] where $M=0$ from $R=0$ to R_{min}. Also "necks" are the locus of a minimum in M and R.
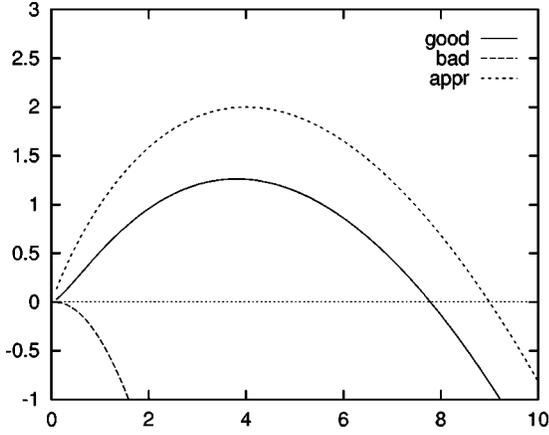
FIG. 1. The function $\psi_H(x)$ for the case $E>0$ with Eq. (3.11) satisfied (middle curve) and with Eq. (3.11) not satisfied (lower curve). The upper curve is the approximating function $\psi_A(x)$ from Eq. (3.12). The parameters (a_1,a_2,t_2-t_1) are (1,2.5,0.5) for the two upper curves and (1,2.5,1.4) for the lower one.

[Writing $\psi_H(x)-\psi_A(x)\equiv\chi_H(x)-(a_2-a_1)x$, and $(\psi_{H,x}-\psi_{A,x})=W(a_2)-W(a_1)$, where $W(a)=a^{3/2}\sqrt{x}/\sqrt{2+ax}-a$, we note that $W(a)$ is a decreasing function of a for every $x>0$, while $\psi_H(0)=\psi_A(0)=0$. Hence, $\psi_H(x)<\psi_A(x)$ for $x>0$.] Therefore, if $\psi_A(x_A)=0$, then $\psi_H(x_A)<0$.

The solution of $\psi_A(x)=0$ is

$$x_A=\frac{(a_2-a_1)^2}{(t_2-t_1)^2},\qquad(3.14)$$

and so x_A is a good initial value for the numerical program that will find a solution of $\psi_H(x)=0$ by bisecting the segment $[0,x_A]$ and checking the sign of $\psi_H(x_A/2)$.

Also, for numerical purposes, the limits of some of the functions at $M=0$ must be calculated separately, as explained in Appendix B.

B. Still-expanding elliptic regions

For $E<0$, a similar result holds, but with one more refinement: depending on the value of (t_2-t_1), the final density will be either in the expansion phase or in the recollapse phase (and only in one of these phases). The dividing value of (t_2-t_1) will come out in the proof below.

Let us assume that the η of Eq. (2.4) is in $[0,\pi]$ for both values of t_i, so that the final density is still in the expansion phase of its evolution. (For $\eta\in[\pi,2\pi]$, the solutions for (t_i-t_B) are different, and they will be considered separately below.) The analogues of Eqs. (3.3) and (3.4) are then

$$t_B=t_i-\frac{M}{(-2E)^{3/2}}[\arccos(1+2ER_i/M)$$

$$-\sqrt{1-(1+2ER_i/M)^2}]\qquad(3.15)$$

and

$$\psi_X(x)=0,\qquad(3.16)$$

where this time

$$x:=-2E/M^{2/3},$$

$$\psi_X(x):=\arccos(1-a_2x)-\sqrt{1-(1-a_2x)^2}$$

$$-\arccos(1-a_1x)+\sqrt{1-(1-a_1x)^2}$$

$$-(t_2-t_1)x^{3/2}:=\chi_X(x)-(t_2-t_1)x^{3/2},\qquad(3.17)$$

the definitions of a_i being still Eq. (3.5).

The reasoning is entirely analogous to the one for Eq. (3.5), but this time the arguments of arccos must have absolute values not greater than 1. This implies $x\leq2/a_i$ for both i, and so, since $a_2>a_1$

$$0\leq x\leq2/a_2,\qquad(3.18)$$

which means: if there is any solution of Eq. (3.16), then it will have the property (3.18). The two square roots in Eq. (3.17) will then also exist. Equation (3.18) is equivalent to the requirement that $(R_{,t})^2$ [in Eq. (2.2) with $\Lambda=0$] is non-negative at both t_1 and t_2.

Note that

$$\psi_X(0)=0,$$

$$\psi_X(2/a_2)=\pi-\arccos(1-2a_1/a_2)$$

$$+2\sqrt{a_1/a_2-(a_1/a_2)^2}$$

$$-(2/a_2)^{3/2}(t_2-t_1),\qquad(3.19)$$

$$\frac{d}{dx}\psi_X(x)=\psi_{X,x}=\sqrt{x}\left[\frac{a_2^{3/2}}{\sqrt{2-a_2x}}\right.$$

$$\left.-\frac{a_1^{3/2}}{\sqrt{2-a_1x}}-\frac{3}{2}(t_2-t_1)\right].\qquad(3.20)$$

In consequence of $a_2>a_1$, the term in square brackets is now an *increasing* function of x, and it becomes $+\infty$ at $x=2/a_2$ [which only means that $\psi_X(x)$ has a vertical tangent there]. Hence, the term can go through zero at most once, and it will do so when it is negative at $x=0$, i.e. when the opposite to Eq. (3.11) holds

$$t_2-t_1>\frac{\sqrt{2}}{3}(a_2^{3/2}-a_1^{3/2}).\qquad(3.21)$$

This means that the model must have expanded between t_1 and t_2 by less than the $E=0$ model would have done. If Eq. (3.21) does not hold, then $\psi_{X,x}$ is positive for all $x>0$, which means that $\psi_X(x)$ is increasing and will not be zero for any $x>0$. Hence, Eq. (3.21) is a necessary condition for the existence of a solution of Eq. (3.16).

With Eq. (3.21) satisfied, $\psi_{X,x}(x)$ becomes negative for some $x>0$, then goes through zero exactly once and then is positive all the way up to $x=2/a_2$. This implies that $\psi_X(x)$ initially decreases below 0, then has exactly one minimum

and is increasing up to the value (3.19) at $x=2/a_2$. Hence, $\psi_X(x)$ will have a zero for $x>0$ only if $\psi_X(2/a_2)\geq 0$, i.e. if

$$t_2-t_1\leq (a_2/2)^{3/2}[\pi-\arccos(1-2a_1/a_2)$$
$$+2\sqrt{a_1/a_2-(a_1/a_2)^2}]. \qquad (3.22)$$

The inequality (3.22) is consistent with Eq. (3.21); see Appendix A. Equations (3.21) and (3.22) together are a necessary and sufficient condition for Eqs. (3.16), (3.17) to define a function $E(M)<0$ for which $R(t_2,M)$ is still in the expansion phase of the model.

C. Recollapsing elliptic regions

The reasoning above applied only in the increasing branch of R in Eq. (2.4). For the decreasing branch, where $\eta \in [\pi,2\pi]$, instead of Eqs. (3.16), (3.17) we obtain

$$t_B=t_1-\frac{M}{(-2E)^{3/2}}[\arccos(1+2ER_1/M)$$
$$-\sqrt{1-(1+2ER_1/M)^2}]$$
$$=t_2-\frac{M}{(-2E)^{3/2}}[\pi+\arccos(-1-2ER_2/M)$$
$$+\sqrt{1-(1+2ER_2/M)^2}] \qquad (3.23)$$

and

$$\psi_C=0, \quad \text{where}$$

$$\psi_C(x):=\pi+\arccos(-1+a_2x)+\sqrt{1-(1-a_2x)^2}$$
$$-\arccos(1-a_1x)+\sqrt{1-(1-a_1x)^2}$$
$$-(t_2-t_1)x^{3/2}. \qquad (3.24)$$

The derivative of this is

$$\frac{d}{dx}\psi_C(x)=\psi_{C,x}=-\sqrt{x}\left[\frac{a_2^{3/2}}{\sqrt{2-a_2x}}+\frac{a_1^{3/2}}{\sqrt{2-a_1x}}\right.$$
$$\left.+\frac{3}{2}(t_2-t_1)\right], \qquad (3.25)$$

and is negative for all $x>0$. Since

$$\psi_C(0)=2\pi>0, \qquad (3.26)$$

the solution of $\psi_C(x)=0$ for $x>0$ will exist if and only if $\psi_C(2/a_2)\leq 0$, which translates into the opposite of Eq. (3.22):

$$t_2-t_1\geq (a_2/2)^{3/2}[\pi-\arccos(1-2a_1/a_2)$$
$$+2\sqrt{a_1/a_2-(a_1/a_2)^2}]. \qquad (3.27)$$
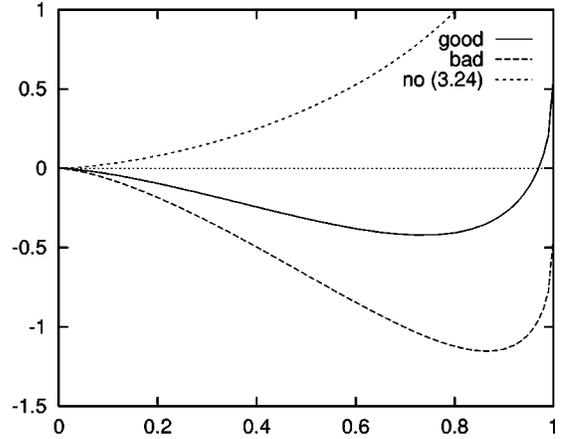
FIG. 2. The function $\psi_X(x)$ for the case $E<0$ with Eqs. (3.21) and (3.22) satisfied (middle curve), with Eq. (3.21) satisfied and Eq. (3.22) not satisfied (lower curve), and with Eq. (3.21) not satisfied (upper curve). The parameters (a_1,a_2,t_2-t_1) are (1,2,2) for the middle curve, (1,2,3) for the lower curve, and (1,2,0.05) for the upper curve.

Thus the two densities can be connected by an $E<0$ LT evolution that is recollapsing at time t_2 if Eq. (3.27) is obeyed.

Examples of functions $\psi_X(x)$ obeying or not obeying Eqs. (3.21) and (3.22), and of functions $\psi_C(x)$ obeying or not obeying Eq. (3.27) are shown in Figs. 2 and 3.

D. Summary

The above analysis considered only single world lines, that is, single M values. We extend this to the whole of $\rho_i(M)$ by noting that $E(M)$ and $t_B(M)$ are arbitrary functions in the LT model, and so continuous ρ_i will generate continuous E and t_B.

The meaning of the limiting cases is now easy to understand. In Eq. (3.11), at M values where $t_2-t_1 =(\sqrt{2}/3)(a_2^{3/2}-a_1^{3/2})$, the final state results from the initial
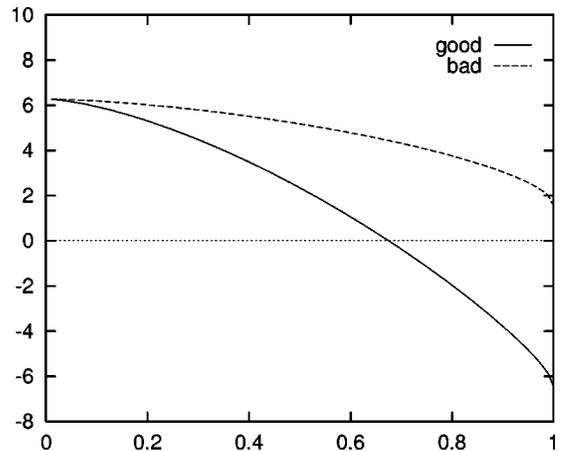
FIG. 3. The function $\psi_C(x)$ from Eq. (3.24) obeying Eq. (3.27) (solid curve) and not obeying it (dashed curve). The parameters (a_1,a_2,t_2-t_1) are (1,2,9) for the first curve and (1,2,0.2) for the other one.

one by a parabolic ($E=0$) evolution, so this M value is on the boundary between an elliptic region and a hyperblic one. Equation (2.5) follows as the $E \to 0$ limit of Eq. (2.4) and of Eq. (2.6). In Eqs. (3.22) and (3.27), for M values where the equality holds, the final state is exactly at the local moment of maximal expansion, separating a region of ρ_2 that is already recollapsing from one that is still expanding.

However, when $E<0$ it must be remembered that the signature of the metric requires that

$$E(M) \geqslant -1/2, \qquad (3.28)$$

and so, once $E(M)$ has been calculated, Eq. (3.28) will have to be checked. Note that the Friedmann model in standard coordinates has exactly this problem—with $2E=-kr^2$ and $M=M_0 r^3$, blindly continuing through $r=1$ will make $E < -1/2$ and $M > M_{Universe}$. Indeed, given two uniform densities $\rho_2 < \rho_1$ that are appropriate for a closed Friedmann model, the integral (3.2) can be extended to arbitrarily large M and R. Thus the occurrence of $E=-1/2$ is not a problem, but rather an indication that the maximum of the spatial section has been reached. One should record the values of R_{max} and M_{max}, and then use

$$R^3_{maxi} - R^3(t_i, M) = \int_M^{M_{max}} \frac{6}{\kappa \rho_i(M')} dM' \qquad (3.29)$$

and distinguish the M values beyond the maximum from those in front of it.

Another serious possibility is that shell crossings, where the density diverges and changes sign, may occur. If they occur between t_1 and t_2 the model evolution is unsatisfactory, but if they occur before t_1 or after t_2, this may not be of much concern. The conditions on $E(M)$ and $t_B(M)$ for avoiding them [7] must also be checked.

All these considerations apply to the Friedmann limit, but it must be remembered that in comparing models in a continuous Friedmann family, one must not scale the curvature index k to $+1$ or -1 when it is nonzero. The parameter k is adapted to the initial and final densities together with M_0. With k scaled to ± 1, taking the limit $k \to 0$ within the family becomes impossible, and the inequalities (3.11) and (3.21) do not come up.

In summary, for densities $\rho_2(M) < \rho_1(M)$ at times $t_2 > t_1$ we have $a_2 > a_1$ where $a_i = R_i/M^{1/3}$, and writing

$$\alpha = a_1/a_2$$

the nature of the LT model that evolves between these states at a given M is:

Hyperbolic $E>0$:
  If

$$t_2 - t_1 < (\sqrt{2} a_2^{3/2}/3)(1 - \alpha^{3/2})$$

then

$$E = xM^{2/3}/2$$

where x solves

$$0 = \psi_H(x) = \sqrt{(1+a_2 x)^2 - 1} - \mathrm{arcosh}(1+a_2 x)$$
$$- \sqrt{(1+a_1 x)^2 - 1} + \mathrm{arcosh}(1+a_1 x) - (t_2 - t_1)x^{3/2}$$

and

$$t_B = t_i - \frac{1}{x^{3/2}} [\sqrt{(1+a_i x)^2 - 1} - \mathrm{arcosh}(1+a_i x)].$$

Parabolic $E=0$:
  If $(t_2 - t_1)$ is close to

$$t_2 - t_1 = (\sqrt{2} a_2^{3/2}/3)(1 - \alpha^{3/2})$$

then a series expansion gives

$$E = xM^{2/3}/2$$

where x solves

$$0 = \psi_P(x) \approx \frac{\sqrt{2} x^{3/2}}{3} \left\{ a_2^{3/2} \left(1 - \frac{3}{20} a_2 x + \frac{9}{224} a_2^2 x^2 \right) \right.$$
$$\left. - a_1^{3/2} \left(1 - \frac{3}{20} a_1 x + \frac{9}{224} a_1^2 x^2 \right) - (t_2 - t_1) \right\}$$

and

$$t_B \approx t_i - \frac{\sqrt{2}}{3} a_i^{3/2} \left(1 - \frac{3}{20} a_i x + \frac{9}{224} a_i^2 x^2 \right).$$

Elliptic $E<0$ and still expanding at t_2:
  If

$$(a_2/2)^{3/2} [\pi - \arccos(1 - 2\alpha) + 2\sqrt{\alpha - \alpha^2}] > t_2 - t_1$$
$$> (\sqrt{2} a_2^{3/2}/3)(1 - \alpha^{3/2})$$

then

$$E = -xM^{2/3}/2$$

where x solves

$$0 = \psi_X(x) = \arccos(1 - a_2 x) - \sqrt{1 - (1 - a_2 x)^2}$$
$$- \arccos(1 - a_1 x) + \sqrt{1 - (1 - a_1 x)^2} - (t_2 - t_1)x^{3/2}$$

and

$$t_B = t_i - \frac{1}{x^{3/2}} [\arccos(1 - a_i x) - \sqrt{1 - (1 - a_i x)^2}].$$

Elliptic $E<0$ and at maximum expansion at t_2:
  If $(t_2 - t_2)$ is close to

$$t_2 - t_1 = (a_2/2)^{3/2} [\pi - \arccos(1 - 2\alpha) + 2\sqrt{\alpha - \alpha^2}]$$

then a series expansion gives

$$E = -xM^{2/3}/2$$

where x solves

$$0 = \psi_M(x) \approx -2^{3/2}(2-a_2x)^{1/2} + \frac{2^{3/2}}{12}(2-a_2x)^{3/2} + \pi$$
$$- \arccos(1-a_1x) + \sqrt{a_1x(2-a_1x)} - x^{3/2}(t_2-t_1)$$

and

$$t_B = t_1 - \frac{1}{x^{3/2}}[\arccos(1-a_1x) - \sqrt{1-(1-a_1x)^2}]$$

$$\approx t_2 - x^{-3/2}\left(\pi - 2^{3/2}(2-a_2x)^{1/2} \right.$$
$$\left. + \frac{2^{3/2}}{12}(2-a_2x)^{3/2} \right).$$

Elliptic $E<0$ and recollapsing at t_2:
   If

$$t_2 - t_1 > (a_2/2)^{3/2}[\pi - \arccos(1-2\alpha) + 2\sqrt{\alpha-\alpha^2}]$$

then

$$E = -xM^{2/3}/2$$

where x solves

$$0 = \psi_C(x) = \pi - \arccos(-1+a_2x) + \sqrt{1-(1-a_2x)^2}$$
$$- \arccos(1-a_1x) + \sqrt{1-(1-a_1x)^2} - (t_2-t_1)x^{3/2}$$

and

$$t_B = t_1 - \frac{1}{x^{3/2}}[\arccos(1-a_1x) - \sqrt{1-(1-a_1x)^2}]$$

$$= t_2 - \frac{1}{x^{3/2}}[\pi + \arccos(-1+a_2x)$$
$$+ \sqrt{1-(1-a_2x)^2}].$$

It is easy to adapt the above for the case $\rho_2 > \rho_1$. Clearly any parabolic or hyperbolic regions would be collapsing.[3]

We conclude this section by stating the result as a theorem:

Theorem. Given any two times t_1 and $t_2 > t_1$, and any two spherically symmetric density profiles $0 < \rho_2(M) < \rho_1(M)$ defined over the same range of M, a LT model can be found that evolves from ρ_1 to ρ_2 in time $t_2 - t_1$. The inequalities (3.11), (3.21) and (3.22), (3.27) will tell which class of LT evolution applies at each M value. The possibilities of shell crossings or excessively negative energies are not excluded, and must be separately checked for.

IV. CONDITIONS FOR COMOVING EXTREMA OF DENSITY

Since we expect the central condensation to propagate outward into the Friedmann background, we have to set up the initial conditions so that the edge of the condensation is not comoving. For this purpose, it is useful to know the general conditions for comoving extrema of density. We shall now consider maxima and minima of ρ in those domains where ρ is differentiable, and use M as the radial coordinate.

From Eq. (2.9) we see that extrema of ρ will occur at those values of M where

$$(R^3)_{,MM} = 0. \tag{4.1}$$

[This is a necessary condition only. Some of the solutions of Eq. (4.1) will be inflection points of $\rho(t_1,M)$ rather than extrema, but the whole reasoning below will apply to them, too.] For the case $E<0$ we find from the second of Eq. (2.4)

$$(1-\cos\eta)\eta_{,M} = \left[\frac{(-2E)^{3/2}}{M} \right]_{,M}(t-t_B) - \frac{(-2E)^{3/2}}{M}t_{B,M}. \tag{4.2}$$

Using this in the first of Eq. (2.4) we find

$$(R^3)_{,MM} = -\left(\frac{M^3}{8E^3} \right)_{,MM}(1-\cos\eta)^3 - 6\left(\frac{M^3}{8E^3} \right)_{,M}(1-\cos\eta)\sin\eta\left\{ \left[\frac{(-2E)^{3/2}}{M} \right]_{,M}(t-t_B) - \frac{(-2E)^{3/2}}{M}t_{B,M} \right\}$$

$$- 3\frac{M^3}{8E^3}\left(\frac{\sin^2\eta}{1-\cos\eta} + \cos\eta \right)\left\{ \left[\frac{(-2E)^{3/2}}{M} \right]_{,M}(t-t_B) - \frac{(-2E)^{3/2}}{M}t_{B,M} \right\}^2$$

$$- 3\frac{M^3}{8E^3}(1-\cos\eta)\sin\eta\left\{ \left[\frac{(-2E)^{3/2}}{M} \right]_{,MM}(t-t_B) - 2\left[\frac{(-2E)^{3/2}}{M} \right]_{,M}t_{B,M} - \frac{(-2E)^{3/2}}{M}t_{B,MM} \right\} = 0. \tag{4.3}$$

---

[3] For an expanding and a collapsing hyperbolic region to be contained in the same smooth model, there would have to be an elliptic region between them. This is because the $\rho_2 < \rho_1$ region and the $\rho_2 > \rho_1$ region must have a point between where $\rho_2 = \rho_1$. The only way this can be arranged without causing shell crossings is for the elliptic region to be a Kruskal-like neck—see [10].

This equation defines certain values of M, let us call them $M = M_{ex}$, at which ρ may have extrema. We will verify when they are comoving, i.e. when M_{ex} are independent of time.

The Jacobian $\partial(M, \eta)/\partial(t, M)$ is nonzero everywhere except those locations where

$$\eta_{,t} = 0 \quad \Rightarrow \quad E = 0. \tag{4.4}$$

Hence, everywhere else M and η can be considered to be independent variables. Using the second of Eq. (2.4), we can eliminate $(t - t_B)$ from Eq. (4.3), and, since the M_{ex} obeying Eq. (4.3) are assumed independent of t, what results is an equation in η with coefficients depending on M. The coefficients of independent functions of η all have to vanish. This implies

$$[(-2E)^{3/2}/M]_{,M} = [(-2E)^{3/2}/M]_{,MM} = t_{B,M} = t_{B,MM} = 0, \tag{4.5}$$

$$(M^3/E^3)_{,MM} = 0, \tag{4.6}$$

all quantities being calculated at $M = M_{ex}$. Equations (4.5) would have the same form in any coordinate system in which $M = M(r)$, but for Eq. (4.6), the coordinate M is privileged; in other coordinates this equation would look less readable. Note that Eqs. (4.5), (4.6) imply that at $M = M_{ex}$ the functions t_B, $[(-2E)^{3/2}/M]$ and (M^3/E^3) agree with their Friedmann values (as determined by $E^{3/2}/M$ and t_B at M_{ex}) up to the second derivatives. This means that the local density is at all times the same as that of the Friedmann model that matches on there.

In brief, we have shown that if $M = M_{ex}$ is an extremum of density, the density is differentiable at M_{ex}, and the extremum is comoving, then Eqs. (4.5), (4.6) are satisfied. Conversely, if ρ is differentiable at M_{ex}, has an extremum there, and Eqs. (4.5), (4.6) are satisfied, then the extremum will be comoving.

By the same method it may be verified that in the $E(M) > 0$ region, where Eq. (2.6) apply, the conditions for a comoving extremum are again of the form (4.5), (4.6), except that now the $(-2E)$ in Eq. (4.5) is replaced by $(2E)$.

For the parabolic case, Eq. (2.5), the condition $(R^3)_{,MM} = 0$ reads

$$-9[(2t_{B,M} + Mt_{B,MM})(t - t_B) - Mt_{B,M}^2] = 0, \tag{4.7}$$

and so the extremum will be comoving when $t_{B,M} = t_{B,MM} = 0$ at $M = M_{ex}$.

Note that for an arbitrary LT perturbation inside an exactly Friedmannian exterior, the density at the boundary may be discontinuous, as in the Einstein-Straus [12,13] configuration. Furthermore, even if it is C^1 at an initial moment, it may develop a discontinuity. However, if the above conditions hold at the boundary, they ensure the density is C^1 through the boundary at all times.

V. NUMERICAL EXAMPLE

A. Scales in the background

The age of the universe is currently believed to be about 14 Gyr. If recombination temperature is ~ 2700 K, then $z = 2700/2.73 \approx 1000$ then recombination happened at about $t_r = 3 \times 10^5$ yr when the density was about 10^{10} times the present density.

However, in a $k = 0$ dust (Friedmann) model, $H_0 = 65$ km/s/Mpc implies $t_0 = 2/3H_0 = 10$ Gyr, which would put t_r at 10^5 yr.

In an LT model that is close to parabolic even today, Eqs. (2.4) and (2.6) require $\sinh \eta - \eta \approx \eta^3/6 \approx \eta - \sin \eta$, so we need $\eta^2 \ll 20$, say $\eta < 0.4$. For a Friedmann model

$$M_F = M_0 r^3, \quad 2E_F = \pm 2E_0 r^2, \quad t_{BF} = 0. \tag{5.1}$$

From Eqs. (2.4) and (2.6) again the limit on E_0 is

$$\frac{(2|E_0|)^{3/2} t_0}{M_0} \approx \frac{\eta^3}{6} < \frac{0.4^3}{6} \approx 0.01. \tag{5.2}$$

In a closed model, the maximum in the spatial sections —the "equator" of the 3-sphere —is at $r = r_m$ where $2E = -1$, so

$$2|E_0| r_m^2 = 1 \quad \Rightarrow \quad r_m = \frac{1}{\sqrt{2|E_0|}} \tag{5.3}$$

at which point the areal radius today is

$$R_{m0} = \left(\frac{9M_0}{2(2|E_0|)^{3/2}} \right)^{1/3} t_0^{2/3}. \tag{5.4}$$

For hyperbolic models, there is no maximum radius, but R_{m0} gives the curvature scale. Another way to restrict E_0 is to specify that the horizon scale ct_0 be much less than R_{m0}, say $t_0 < R_{m0}/8$, which gives a restriction similar to Eq. (5.2).

A third way to limit E_0 is to specify $\Omega_0 > 0.03$. In a hyperbolic model

$$\Omega = \frac{8\pi\rho R^2}{3\dot{R}^2} = \frac{2}{1 + \cosh(\eta)}. \tag{5.5}$$

Solving this for η and using Eq. (2.6) again gives

$$\frac{(2|E_0|)^{3/2} t_0}{M_0} < 0.016. \tag{5.6}$$

However, within a condensation, the evolution may be nowhere near parabolic.

B. Past null cones, horizons and scales on the CMB sky

The physical radius of the past null cone in a $k = 0$ Friedmann dust model with scale factor $S \propto t^{2/3}$ is

$$L(t) = S \int_t^{t_0} \frac{1}{S} dt = 3c(t_0^{1/3} t^{2/3} - t) \tag{5.7}$$

so an observed angular scale of θ on the CMB sky has a physical size at recombination of

$$L_r = L(t)\theta = 3c(t_0^{1/3}t_r^{2/3} - t_r)\theta. \tag{5.8}$$

The present day size of the observed structure—assuming it does not collapse—is merely scaled up by the ratio of scale factors

$$L_0 = L_r \frac{S_0}{S_r}. \tag{5.9}$$

The scales would be fairly similar in reasonable $k \neq 0$ models.

To determine the condensed structures that correspond to a given present day scale in the background, the mass M_c of the condensation is divided by the present day density $\rho_{b,0}$ of the Friedmann background ($k=0$ dust) and cube-rooted:

$$L_{c0} = \left(\frac{3M_c}{4\pi\rho_{b,0}}\right)^{1/3}. \tag{5.10}$$

Conversely, the mass associated with a given scale at a given time is

$$M_c = \frac{4\pi L_c(t)^3 \rho_b(t)}{3}. \tag{5.11}$$

The particle (causal) horizon at any given time t is

$$C = S\int_0^t \frac{1}{S}dt = 3ct \tag{5.12}$$

and the visual horizon is

$$V = S\int_{t_r}^t \frac{1}{S}dt = 3c(t - t_r^{1/3}t^{2/3}). \tag{5.13}$$

The particle horizon takes no account of inflation, and retains a dust equation of state before recombination, so is only included as a rough scale of interest.

C. Scales in the perturbation

We imagine that present day structures accreted their mass from a background that was close to Friedmannian, and therefore the scale of the matter that is destined to end up in a present day condensation is fixed by its present day mass.

The Cosmic Background Explorer (COBE) data shows $\delta T/T \sim 10^{-5}$ on scales of $10°$, and the density perturbations are $\delta\rho/\rho = 3\,\delta T/T \lesssim 3\times10^{-5}$ [15]. The power spectrum $\mathcal{P}(k) = |\delta_{\mathbf{k}}|^2 =$ where $\delta\rho/\rho = \Sigma_{\mathbf{k}}\delta_{\mathbf{k}}e^{i\mathbf{k}\cdot\mathbf{x}}$ is commonly approximated by $\mathcal{P}(k) = Ake^{-ks}$, where the cutoff scale s is small compared to the Hubble scale. This is just $\mathcal{P} = Ak$ at longer wavelengths (smaller k) [16]. COBE's measurements had a resolution of $\sim 10°$, while BOOMERANG's and MAXIMA's were $\sim 0.2°$. These angular scales correspond to length scales of 2 Mpc and 50 kpc at the time of decoupling, and thus to 2 Gpc and 50 Mpc today. Thus we are only just beginning to detect void scale perturbations in the CMB.

TABLE I. Approximate scales associated with present day structures. Note that the horizons are those in $k=0$ Friedmann models without inflation, as given in Sec V B. The masses associated with the resolution scales of COBE, MAXIMA and BOOMERANG are obtained by assuming a density equal to the parabolic background value ρ_b, as indicated by "(1)" in the density column. Useful collections of data can be found at the following web addresses: http://www.obspm.fr/messier/, http://adc.gsfc.nasa.gov/adc/sciencedata.html, and http://www.geocities.com/atlasoftheuniverse/supercls.html

	Radius today (kpc)	Mass ($M_\odot$)	Density of sphere (ρ_b)	Angle on CMB sky (°)
Star	2×10^{-11}	1	2×10^{29}	8×10^{-7}
Globular cluster	0.1	10^5	2×10^5	4×10^{-5}
Galaxy	15	10^{11}	6×10^4	4×10^{-3}
Virgo cluster	2000	2×10^{13}	5	0.02
Virgo supercluster	15 000	5×10^{14}	0.3	0.06
Abell cluster (example)	800	10^{15}	4000	0.08
Void	6.10^4	?		0.4
Recomb horizon	280			1.8
Present horizon	9.2×10^6			59
Visual horizon	8.9×10^6			57
COBE resolution	1.6×10^6	1.9×10^{21}	(1)	10
BOOM/MAX resolution	3.1×10^4	1.5×10^{16}	(1)	0.2

Although the magnitude of galaxy scale or even supercluster scale perturbations, are not yet directly constrained by observations, we will retain the figure of $\sim 10^{-5}$.

The scales associated with present day structures are summarized in Table I.

D. Choice of units and scales

For the background Friedmann model, we choose the simplest case, as its only purpose it to get the cosmic time scales and densities approximately right:

$$\Lambda = 0, \quad k = 0, \quad p = 0. \tag{5.14}$$

We will use geometric units such that $c = 1 = G$, and the remaining scale freedom of GR is fixed by choosing units in which the present day mass of the condensation being considered is 1. The corresponding geometric length and time units are then

$$M_G = 1 \quad \Rightarrow \quad L_G = M_G G/c^2, \quad T_G = M_G G/c^3. \tag{5.15}$$

E. The model

The principal limitation of the LT model in the post-recombination era is the absence of rotation. However, once rotation has become a significant factor in the collapse process, there is already a well defined structure. Later on pressure and viscosity will become important. Our interest is in
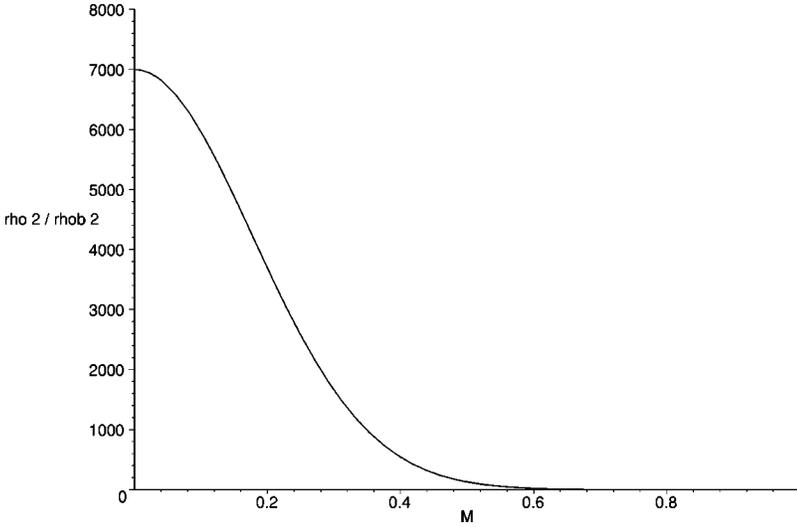
FIG. 4. The chosen density profile $\rho_2(M)/\rho_{b,2}$ as a multiple of the "background" density, for an Abell cluster at time $t_2 = 10$ Gyr. The axes are in geometric units such that $M_{Abell\ cluster} = 1$, as given in Eqs. (5.15) and (5.18).

generating highly condensed structures in a short enough time scale, and these factors only come into play once collapse is well underway. Because of the lack of rotation, etc., all of which tend to delay or halt collapse, we expect our model to be rapidly collapsing rather than stationary at the present day.

We choose to model an Abell cluster:

$$M_{Abell\ cluster} = 10^{15}\ M_\odot. \tag{5.16}$$

$$R_{Abell\ cluster} = 800\ \text{kpc}. \tag{5.17}$$

From Eq. (5.15) and Table I the associated geometric units are

$$1\ M_G = M_{Abell\ cluster}$$

$$1\ L_G = 48\ \text{pc}$$

$$1\ T_G = 156\ \text{yr}$$

$$\rightarrow M_{Abell\ cluster} = 1\ M_G$$

$$R_{Abell\ cluster} = 16800\ L_G$$

$$t_2 = 6.4 \times 10^7 T_G. \tag{5.18}$$

1. Final profile

At $t_2 = 10$ Gyr$= 6.4 \times 10^7 T_G$, we specify the density profile to be

$$\rho_2(M) = \rho_{b,2}(7000\,e^{-(4M)^2}) \tag{5.19}$$

which is shown in Fig. 4. Now the Friedmann density at t_2 is

$$\rho_{b,2} = 1.3 \times 10^{-17} M_G/L_G^3 = 8 \times 10^{-27}\ \text{kg/m}^3 \tag{5.20}$$

so the radius in the Friedmann "background" that contains this mass is[4]

$$R_{F,2} = \left(\frac{3M_{Abell\ cluster}}{4\pi\rho_{b,2}}\right)^{1/3} = 260\,000\,L_G. \tag{5.21}$$

Thus we find

$$(R_2(M))^3 = \int_0^M \frac{3}{4\pi\rho_2(M')}\,dM' = \frac{3}{224\,000\sqrt{\pi}\rho_{b,2}}\,\text{erfi}(4M) \tag{5.22}$$

as shown in Fig. 5, and the resulting $\rho_2(R)$ is shown in Fig. 6.

2. Initial profile

At $t_1 = 100$ k yr$= 10^{-5}t_2 = 641\,T_G$ we specify the density perturbation to have mass

$$M_1 = 10^{-2}M_{Abell\ cluster} \tag{5.23}$$

and density enhancement

$$3 \times 10^{-5}\rho_{b,1} \tag{5.24}$$

for which the chosen profile is

$$\rho_1(M) = \rho_{b,1}\left(\frac{1.00003(1+100\,M)}{1+100.003\,M}\right) \tag{5.25}$$

as plotted in Fig. 7. The Friedmann density at t_1 is

$$\rho_{b,1} = 1.3 \times 10^{-7}\ M_G/L_G^3 = 8 \times 10^{-17}\ \text{kg/m}^3 \tag{5.26}$$

_____

[4]For backgrounds with $k \neq 0$, the radius that contains this mass would be adjusted slightly.
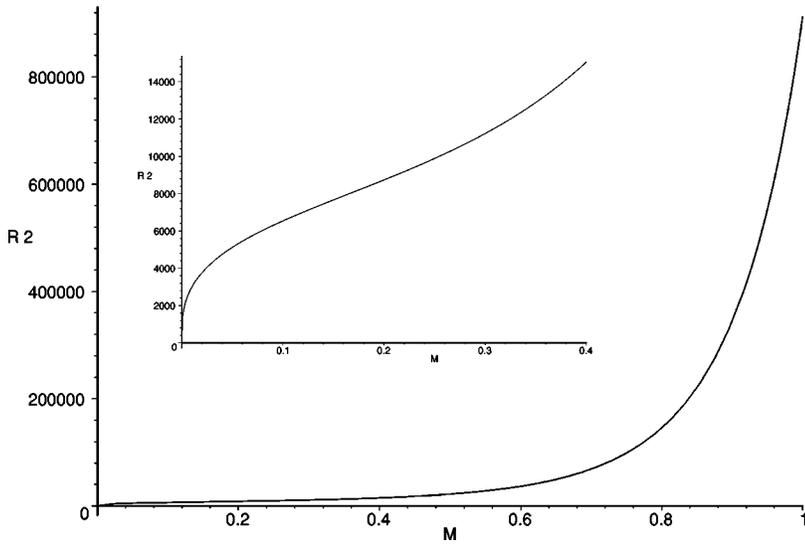
FIG. 5. The areal radius $R_2(M)$ at time t_2, that results from the chosen $\rho_2(M)$. The inset shows an enlargement of the curve near small M. The axes are in geometric units.
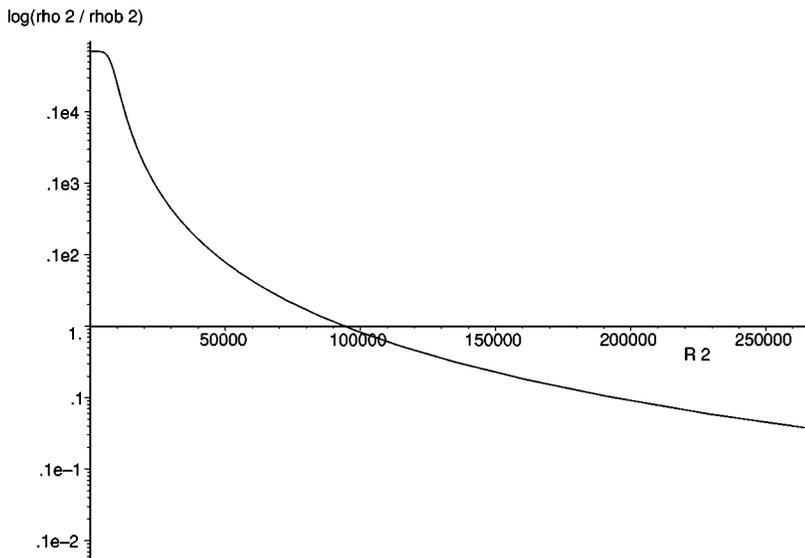
FIG. 6. The density profile $\rho_2/\rho_{b,2}$ against areal radius R_2. The axes are in geometric units.
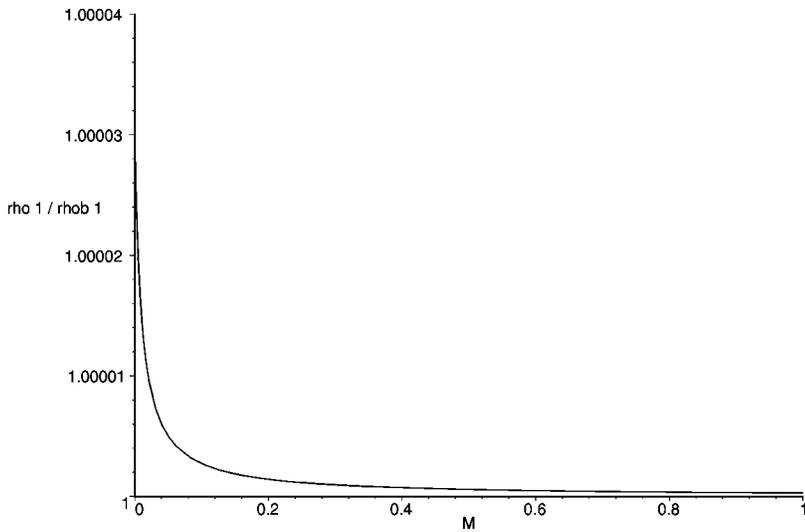
FIG. 7. The density profile $\rho_1(M)/\rho_{b,1}$ chosen for the initial perturbation at time t_1. The axes are in the geometric units of Eqs. (5.15) and (5.18).
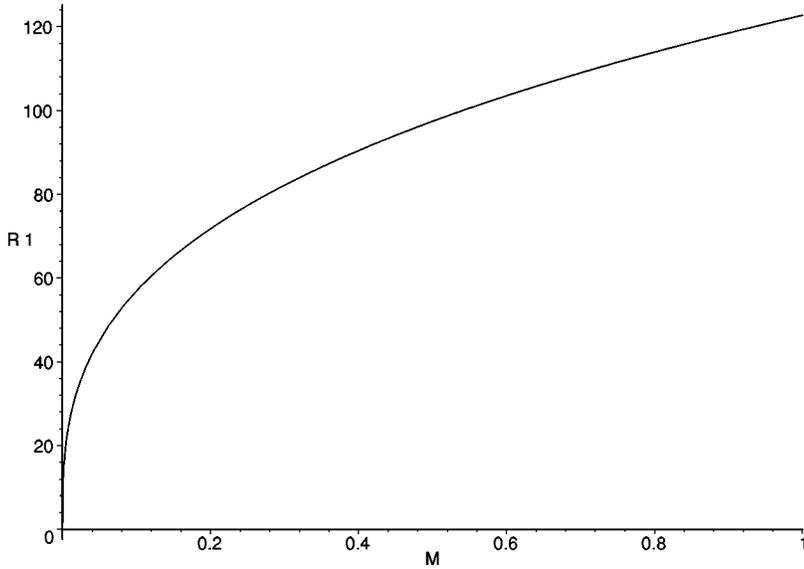
FIG. 8. Areal radius $R_1(M)$ at time t_1, that is obtained from $\rho_1(M)$. The axes are in geometric units.

and the radius in the "background" that contains the total mass is

$$R_{F,1} = \left(\frac{3 M_{Abell\ cluster}}{400 \pi \rho_{b,1}} \right)^{1/3} = 26\ L_G. \qquad (5.27)$$

The resulting $R_1(M)$,

$$(R_1(M))^3 = \int_0^M \frac{3}{4 \pi \rho_1(M')} dM'$$

$$= \frac{3}{4 \pi \rho_{b,1}} \left(M - \frac{0.00003}{100.003} \ln(1 + 100\,M) \right) \qquad (5.28)$$

is shown in Fig. 8, and $\rho_1(R)$ in Fig. 9.

F. Model results

A Maple program was written to generate the formulas and then solve for $E(M)$ and $t_B(M)$ numerically, as explained in Sec. III. The results are shown in Figs. 10 and 11.

We see that E is of order 10^{-5} which gives a recollapse time scale of $10^7\ T_G = 1.7 \times 10^9$ yr, so that the curvature in the condensation is of order $M t_2 / (2E)^{3/2} \sim 0.17$. The bang time perturbation is of order $2\ T_G = 300$ yr, and is quite negligible.

Strictly speaking, an increasing t_B, $t_{B,M} > 0$, creates a shell crossing, but for such a slight variation in t_B, the shell crossing occurs very early on, long before t_1 when the model becomes valid.

The "velocity" $R_{,t}$—rate of change of the areal radius R—would, in a homogeneous model, increase as $M^{1/3}$, so plotting $R_{,t}/M^{1/3}$, as in Fig. 12, indicates the velocity perturbation, as a deviation from a constant value.

In this case, the perturbation is within 3×10^{-5} for $0 < M < 0.6$, where ρ_2 is large, but increases to 8×10^{-4} in the near vacuum region $0.6 < M < 1$. This slight excess is most
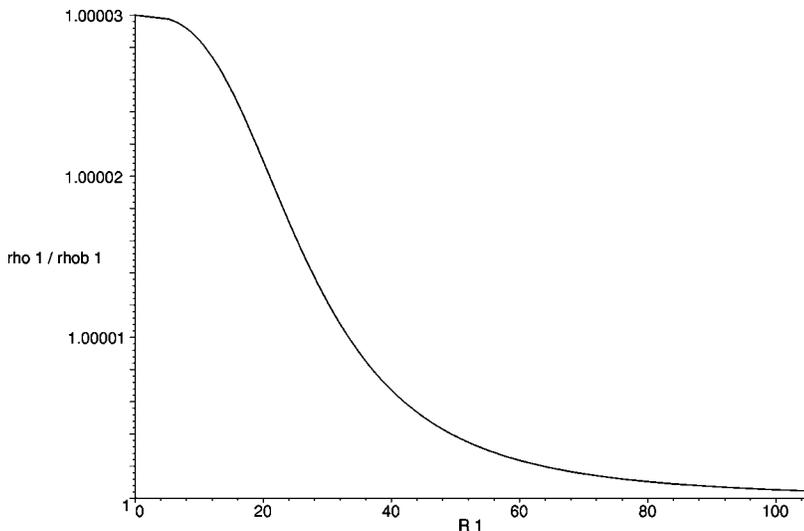
FIG. 9. Density profile $\rho_1/\rho_{b,1}$ against areal radius R_1. The axes are in geometric units.
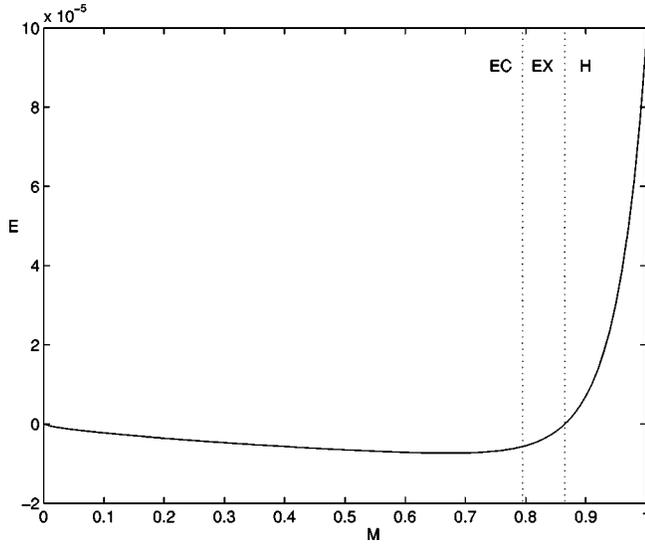
FIG. 10. The LT energy function $E(M)$ obtained from solving for the LT model that evolves between $\rho_1(M)$ and $\rho_2(M)$. The axes are in geometric units. The symbols "EC," "EX," and "H" indicate regions that are respectively elliptic and recollapsing at t_2 (EC), elliptic and still expanding at t_2 (EX), and hyperbolic (H).

likely due to choosing a $\rho_2(M)$ that falls off too fast outside the condensation, requiring a too strongly hyperbolic evolution that expands too rapidly. It is likely that this same effect requires the slightly increasing t_B to keep $\rho_1(M)$ almost flat in these outer regions.

As a cross-check, these derived functions were used in a separate MATLAB program that plots the evolution of a LT model, given its arbitrary functions. (The appropriate form of the evolution equations is given in Appendix B.) The initial and final density profiles were recovered to high accuracy. The resulting density evolution is shown in Fig. 13.
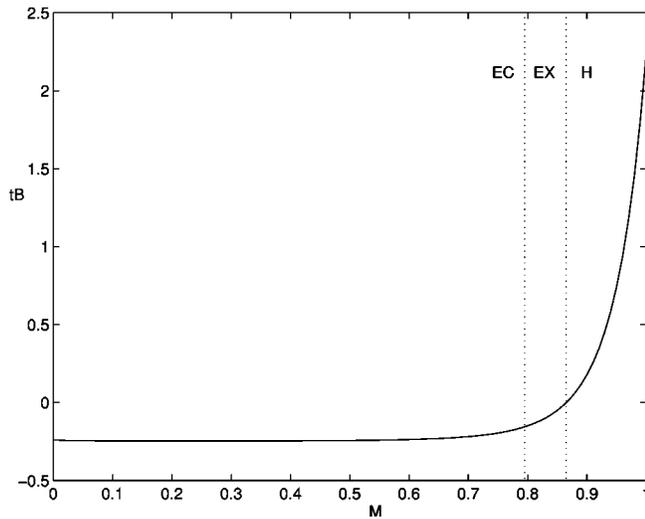
FIG. 11. The LT bang time function $t_B(M)$ obtained from solving for the LT model that evolves between $\rho_1(M)$ and $\rho_2(M)$. The axes are in geometric units.
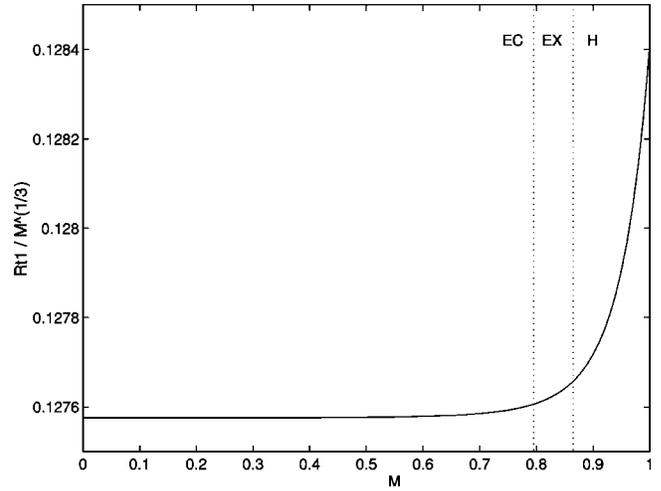
FIG. 12. The velocity perturbation $\dot{R}/M^{1/3}$ at time t_1. A constant value would indicate no perturbation. The axes are in geometric units.

VI. CONCLUSIONS

We proved that an LT model can be found to evolve any initial density profile on a constant time slice, to any final density profile a given time later. Although it cannot be guaranteed the resulting model is free of physical singularities such as shell crossings, and the occurrence of a large negative energy ($E = -1/2$) must be handled correctly by changing to M and R decreasing, our numerical experiments indicate that realistic choices of the two density profiles and the time difference are likely to generate reasonable models.

Our numerical example created an Abell cluster in a real-
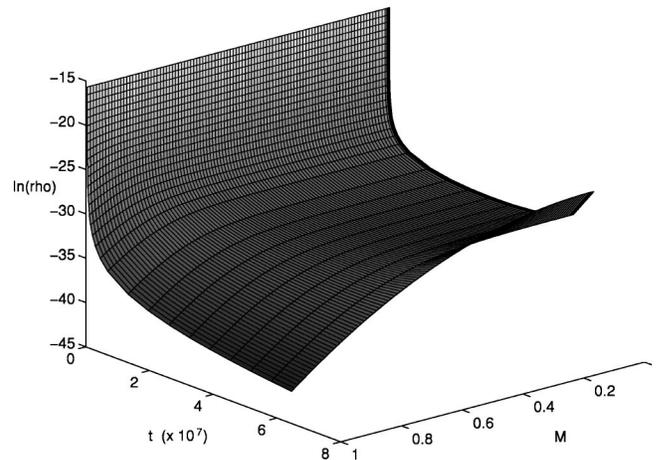
FIG. 13. The evolution of $\rho(t,M)$ for the derived LT model. The axes are in the geometric units of Eqs. (5.15) and (5.18). In the range $0 < M < 0.795$ the evolution is elliptic and already recollapsing at time t_2, in $0.795 < M < 0.865$ it is elliptic but still expanding at t_2, and for $M > 0.865$ it is hyperbolic. In practice, recollapse would be halted at some point by the effects of pressure, rotation, etc. The initial and final density profiles calculated at times t_1 and t_2 coincide with those originally chosen and shown in Figs. 7 and 4, respectively.

istic time scale. It started from recombination, with a density perturbation involving a small amount of mass, having $\delta\rho/\rho \sim 3 \times 10^{-5}$. It then "accreted" most of its final mass. In fact this "accretion" consists of lower expansion rates near the center, and more rapid expansion rates further out. Only at late stages does actual collapse begin at the center. The initial velocity perturbation cannot be chosen if the initial and final densities are chosen. It turned out to be $\delta v/v \sim 3 \times 10^{-5}$ within the future condensation and $\sim 8 \times 10^{-4}$ in the future vacuum region. The relatively large value in the outer regions is probably due to choosing the final density profile, ρ_2 to fall off more rapidly than ideal.

The preceding two points—the theorem plus the numerical example—demonstrate that the LT model provides a very reasonable description of post-recombination structure formation.

These two points also indicate that post recombination structure formation in a dust universe has an important kinematical component—the initial distribution of velocities has as much bearing on whether or not a condensation forms and gravity magnifies density fluctuations, as the initial density distribution. These initial distributions of density and velocity are generated by the functions $E(M)$ and $t_B(M)$, i.e., coded in the initial conditions.

Further numerical examples for structure formation on a variety of scales within the LT model are under investigation.

We also obtained the conditions for a density maximum or minimum or shoulder to be comoving. Since these are resitrictions on the LT arbitrary functions, it is evident that extrema are in general moving through the fluid, as argued in [17], and are not comoving. In other words present day density maxima are not likely to be on the same world lines as initial density maxima.

APPENDIX A: CONSISTENCY OF THE INEQUALITIES (3.21) AND (3.22)

The inequalities (3.21) and (3.22) will be consistent if the right-hand side of Eq. (3.21) is smaller than the right-hand side of Eq. (3.22) in the whole range of a_1 and a_2, i.e. when

$$\frac{\sqrt{2}}{3}(a_2{}^{3/2} - a_1{}^{3/2}) < (a_2/2)^{3/2}[\pi - \arccos(1 - 2a_1/a_2)$$

$$+ 2\sqrt{a_1/a_2 - (a_1/a_2)^2}]. \quad (A1)$$

Defining $y = a_1/a_2$, and recalling that $a_2 > a_1 > 0$ by assumption, the above is equivalent to

$$f(y) > 0 \quad \text{for all } 0 < y < 1, \text{ where}$$

$$f(y) := \pi - \arccos(1 - 2y) + 2\sqrt{y - y^2} - \frac{4}{3}(1 - y^2).$$
$$(A2)$$

Now observe that

$$f(0) = \pi - \frac{4}{3} > 0, \quad f(1) = 0,$$

$$\frac{df}{dy} = 2\frac{\sqrt{y}}{\sqrt{1 - y^2}}(\sqrt{1 - y} - 1) < 0.$$
$$(A3)$$

Hence, $f(y)$ is monotonically decreasing from $f(0) > 0$ to 0 and so is positive for all $0 < y < 1$, which proves Eq. (A1).

APPENDIX B: NUMERICAL CONSIDERATIONS

1. Limiting values at $M = 0$

Several of the quantities considered in this paper have the value 0 at the center of symmetry, where $M = 0$. The variables used in the proof of the theorem, a_i and x, have finite limits as $M \to 0$. For numerical programs, these limiting values have to be provided explicitly.

The values of a_i at $M = 0$ follow very easily. Since $a_i = R(t_i, M)/M^{1/3}$ and $R^3 = \int_0^M [6/\kappa\rho(t,x)]dx$, we have, applying l'Hôpital's rule in the third step

$$a_i(0) = \lim_{M \to 0} \frac{R(t_i, M)}{M^{1/3}} = \left[\lim_{M \to 0}\left(\frac{R^3}{M}\right)\right]^{1/3}$$

$$= \left(\lim_{M \to 0}\frac{d}{dM}R^3\right)^{1/3} = \left(\lim_{M \to 0}\frac{6}{\kappa\rho}\right)^{1/3}$$

$$= \left(\frac{6}{\kappa\rho(t_i, 0)}\right)^{1/3}. \quad (B1)$$

The variable x comes out nonzero automatically when nonzero values of $a_i(0)$ are used in the program; this follows from the proof of the theorem in Sec. III.

2. Practical variables

In practice, it was convenient to define $\alpha = a_1/a_2$, $z_i = t_i/a_2$, and $y = a_2 x$, and then solve the various $\psi = 0$ equations in terms of the variable y, since a_2 was in general quite large, whereas $0 < ax < 2$ in elliptic regions, and ax was at most 200 in a quite strongly hyperbolic region.

3. Reconstructing the model evolution

For reconstructing the evolution of the model, it is convenient to re-write the LT solutions in terms of x and a.

Elliptic:

$$R = M^{1/3} \frac{(1 - \cos \eta)}{x}, \quad t - t_B = \frac{(\eta - \sin \eta)}{x^{3/2}}, \quad \dot{R} = M^{1/3} \sqrt{x \left(\frac{2}{1 - \cos \eta} - 1 \right)}.$$

Parabolic or close to it:

$$R = M^{1/3} \left(\frac{9}{2} \right)^{1/3} (t - t_B)^{2/3} \left(1 + \frac{x}{20} [6(t - t_B)]^{2/3} - \frac{3x^2}{2800} [6(t - t_B)]^{4/3} + \frac{23x^3}{504000} [6(t - t_B)]^2 \right)$$

$$\dot{R} = M^{1/3} \sqrt{4 [6(t - t_B)]^{-2/3} \left(1 + \frac{x}{5} [6(t - t_B)]^{2/3} + \frac{x^2}{280} [6(t - t_B)]^{4/3} - \frac{x^3}{3600} [6(t - t_B)]^2 \right)}. \tag{B2}$$

Hyperbolic:

$$R = M^{1/3} \frac{(\cosh \eta - 1)}{x}, \quad t - t_B = \frac{(\sinh \eta - \eta)}{x^{3/2}}, \quad \dot{R} = M^{1/3} \sqrt{x \left(\frac{2}{\cosh \eta - 1} + 1 \right)}.$$

In all cases the density is

$$\rho = \frac{1}{4 \pi a^2 (a/3 + M a_{,M})}.$$

[1] A. Krasiński, *Inhomogeneous Cosmological Models* (Cambridge University Press, Cambridge, England, 1997).

[2] W.B. Bonnor, Z. Astrophys. **39**, 143 (1956); reprinted in Gen. Relativ. Gravit. **30**, 1113 (1998).

[3] G. Lemaître, Ann. Soc. Sci. Bruxelles **A53**, 51 (1933); reprinted in Gen. Relativ. Gravit. **29**, 641 (1997).

[4] R.C. Tolman, Proc. Natl. Acad. Sci. U.S.A. **20**, 169 (1934); reprinted in Gen. Relativ. Gravit. **29**, 935 (1997).

[5] P. Szekeres, Commun. Math. Phys. **41**, 55 (1975).

[6] S.W. Goode and J. Wainwright, Phys. Rev. D **26**, 3315 (1982).

[7] C. Hellaby and K. Lake, Astrophys. J. **290**, 381 (1985); **300**, 461(E) (1985).

[8] W.B. Bonnor, Phys. Lett. **112A**, 26 (1985).

[9] A. Barnes, J. Phys. A **3**, 653 (1970).

[10] C. Hellaby, Class. Quantum Grav. **4**, 635 (1987).

[11] I.D. Novikov, Vestn. Mosk. Univ., Fiz., Astron. no. 5, 90 (1962).

[12] A. Einstein and E.G. Straus, Rev. Mod. Phys. **17**, 120 (1945).

[13] A. Einstein and E.G. Straus, Rev. Mod. Phys. **18**, 148 (1946).

[14] W.B. Bonnor and A. Chamorro, Astrophys. J. **361**, 21 (1990).

[15] T. Padmanabhan, *Cosmology and Astrophysics Through Problems* (Cambridge University Press, Cambridge, England, 1996).

[16] P.J.E. Peebles, *Principles of Physical Cosmology* (Princeton University Press, Princeton, NJ, 1993).

[17] G.F.R. Ellis, C. Hellaby, and D.R. Matravers, Astrophys. J. **364**, 400 (1990).